

Throughput/Delay Measurements of Limited Feedback Beamforming for Indoor Wireless Networks

Robert C. Daniels, Ketan Mandke, Kien T. Truong, Scott Nettles, and Robert W. Heath, Jr.
 {rdaniels, mandke, ktruong, nettles, rheath}@ece.utexas.edu
 Wireless Networking and Communications Group
 Dept. of Electrical and Computer Engineering
 The University of Texas at Austin

Abstract—In this paper we observe the tradeoff between throughput and feedback delay of limited feedback beamforming in indoor wireless channels with a practical MIMO-OFDM prototype. Past results are largely based on simplified models of the wireless channel. Unfortunately, wireless channel models may not accurately represent the complexities in a real wireless channel such as frequency offset, phase noise, and ambient interference. Furthermore, system impairments, including channel estimation error and synchronization error, only exacerbate the problem of modeling a real wireless system. One such analytical result [1] predicts the performance of limited feedback beamforming as an exponential function of feedback delay. This analytical result has been confirmed through Monte Carlo simulation under Rayleigh fading channel models. Through rigorous measurements and experimentation this paper both evaluates the performance of limited feedback beamforming under feedback delay and confirms the accuracy of the analytical results. Moreover, we give some insights into the methodology for conducting such experiments.

Index Terms—MIMO, Beamforming, Feedback Delay, Limited Feedback, Wireless Experimentation, IEEE 802.11n

I. INTRODUCTION

Multiple-input multiple-output (MIMO) wireless systems employ multiple antennas at both the transmitter and the receiver to offer higher data throughput and reliability than single-antenna links. MIMO transmission technologies fall into two distinct categories: diversity strategies that improve reliability and spatial multiplexing strategies that increase rate. For the experiments conducted in this work, we will focus on a diversity strategy that uses channel state information (CSI) at the transmitter, namely beamforming. By aligning the transmitted signal with the dominant eigenmode of the MIMO channel matrix, beamforming techniques allow MIMO systems to obtain full diversity order and increase the channel capacity with low complexity receiver structures [2], [3].

Beamforming requires the availability of channel state information at the transmitter. In the absence of perfect channel

knowledge at the transmitter, the CSI can be quantized at the receiver and sent back to the transmitter using a low-rate feedback channel [4]. This technique is known as *limited feedback*. Different types of limited feedback for beamforming have been developed [5], [6], [7]. It was also shown that limited feedback beamforming systems with only 5 or 6 feedback bits can obtain the performance very close to unquantized beamforming systems [5], [8].

Most prior work on limited feedback beamforming assumes that the feedback channel is zero-delay such that instantaneous CSI can be delivered to the transmitter. In practical systems, however, the existence of feedback delay is inevitable due to signal processing and transmission delays. Because of the time-varying nature of the wireless channel, feedback delay can cause a mismatch between CSI at the transmitter and the actual channel state. In other words, feedback delay decreases the performance of limited feedback beamforming systems.

Although beamforming with CSI at the transmitter has been well studied it has only recently been introduced into next generation wireless standards, notably IEEE 802.11n and WiMax. One critical aspect of beamforming that is not well understood is performance degradation due to feedback delay. Analytical results have characterized this tradeoff through limited feedback beamforming [1], however, the channel model used to derive analytical results does not necessarily represent the dynamics of a real wireless channel. This paper, through exhaustive measurements of throughput, confirms this analytical result for predicting the effects of feedback delay. We not only verify, but also show that simple measurements can characterize the feedback delay tradeoff, thus avoiding extensive measurement campaigns as conducted in this paper.

The use of Hydra, a flexible, software-defined wireless prototype, considerably reduced the complexity of the substantial experiments performed in this paper. First, the programmable physical layer, based on IEEE 802.11n, allowed for experiments to implement multiple limited feedback beamforming strategies. Additionally, Hydra's implementation on a general purpose processor (GPP) allows us to utilize existing networking protocols to establish a reliable, low-latency feedback channel. This GPP platform also simplifies the data logging procedure, a significant aspect of experimentation.

Physical experimentation is not often used for performance

This material is based in part upon work supported by the National Science Foundation under grants EIA-0322957, CNS-0435307, and CNS-0626797, the Air Force Research Lab under grant numbers FA8750-06-1-0091, and FA8750-05-1-0246, the Office of Naval Research under grant number N00014-05-1-0169, and the DARPA IT-MANET program, Grant W911NF-07-1-0028.

evaluation in wireless communications research. This paper includes a rigorous and detailed explanation of all the procedures used in our experiments. This documentation can be used by other investigators to independently verify our claims. Moreover, this detailed approach provides a reference for future wireless communications and limited feedback experiments.

The remainder of the paper will be organized as follows. Section II provides a literature review on this topic to highlight the paper's contributions. Section III will describe, in detail, the Hydra prototype used to conduct the feedback experiments. Section IV presents the experimental setup including characteristics of the wireless channel observed, testing procedures, and relevant hardware settings. Given this experimental setup, Section V profiles the system performance of beamforming and limited feedback beamforming with feedback delay.

Notation: \mathbb{R} and \mathbb{C} designate the real and complex fields, respectively. Scalars that have variable values are given lowercase letters, x , whereas system-wide scalar values are assigned uppercase letters, X . A random variable X with uniform distribution is presented by stating $X \sim \mathcal{U}[a, b]$ where $a, b \in \mathbb{R}$ represent the upper and lower bound, respectively, on the support of the uniform distribution. The multidimensional real and complex fields, i.e. matrix space, use the notation $\mathbb{R}^{m \times n}$ and $\mathbb{C}^{m \times n}$ such that matrices in this space have m rows and n columns. Bold uppercase letters \mathbf{A} denote matrices. The transpose of matrix \mathbf{A} is labeled \mathbf{A}^T and the Hermitian transpose is given by \mathbf{A}^H . If a matrix \mathbf{A} is reduced to a single column or row matrix it will be observed as a lowercase bold letter \mathbf{a} , which is also the notation for all vectors in this paper. Row x or column y of matrix \mathbf{A} is specified by $[\mathbf{A}]_{x,:}$ or $[\mathbf{A}]_{:,y}$, respectively. Similarly, the entry of matrix \mathbf{A} at row x and column y is stated as $[\mathbf{A}]_{x,y}$. Finally, adopting engineering notation, $j = \sqrt{-1}$.

II. RELATED WORK

The Markov chain model is used in [9] and [1] for modeling the channel state evolution and deriving the theoretical capacity of MIMO systems in the presence of feedback delay. Both papers show that the theoretical capacity of MIMO systems degrades when the CSI is not timely updated at the transmitter. Moreover, in [1], the authors show that the capacity gain decay rate is upper-bounded by an exponential function of delay. Although not in the context of limited feedback context, some related studies are conducted in [10], [11], [12]. An algorithm to determine the maximum tolerable channel feedback delay with capacity loss of at most 5% for each particular channel realization in MIMO systems is proposed in [10]. In [11], it is shown that improved beamforming vectors may be designed by exploiting the effect of feedback delay in the beamforming vector design. Results in [12] show that the assumption of perfect CSI still works well in an adaptive modulation system with delayed error-free feedback channel if the feedback delay $\tau \leq 0.01/f_d$, where f_d denotes the Doppler frequency.

All of the above feedback delay results are based on some model of the temporal correlation in the wireless channel. It is nearly impossible to simulate physical features of devices and channels in real wireless systems. There exist very few

TABLE I
RF/BASEBAND HARDWARE SPECIFICATION FOR EXPERIMENTS

Specification	Value
Operating Frequency	2.5 GHz
Maximum Transmit Power	10 mW
Symbol Rate	1 MHz [†]
Antenna Type	L-shaped Microstrip
Antenna Reflection Coefficient	< -20 dB
Number of Receive Antennas	2
Number of Transmit Antennas	2

[†] Although the USRP supports 20 MHz sampling rates, the bandwidth is constrained by the USB 2.0 interface.

feedback delay results based on experimental performance analysis [13]. Just as in [14] and [15], the focus of [13] is, however, on the performance of channel prediction method that predicts CSI when the signals are transmitted at the receiver and feeds the predicted CSI back to the transmitter. Moreover, even for testbed-based evaluation methods, to get correct results, it is important to characterize the physical features of the specific hardware and environment used in the experiment, namely: ambient interference, RF hardware impairments, and fading properties of wireless channel [16].

III. SYSTEM DESCRIPTION

All limited feedback beamforming experiments in this paper were conducted on the Hydra MIMO-OFDM multihop network prototype at the University of Texas at Austin. Designed for cross-layer wireless communications research, the Hydra prototype allows for flexibility in several layers of the communication system. At the top level, Hydra consists of a general purpose PC interfacing with the Universal Software Radio Peripheral (USRP) hardware [17]. The USRP board implements the RF and analog-to-digital/digital-to-analog conversion. The USRP connects to the general purpose processor (e.g. a Linux machine) through a USB 2.0 interface. Because nearly all of the digital signal processing is done on the general purpose processor, Hydra benefits from a highly configurable architecture in the physical layer algorithms (PHY) to the medium access control layer (MAC) and all layers above. The remainder of this section is dedicated to reviewing the RF hardware specifications, the system architecture constraints, and the current PHY implementation. Since the experiments conducted in this paper do not take advantage of the MAC implemented in Hydra, we will not discuss its contents here. The reader, however, is encouraged to see [18], [16], [19] for a more detailed discussion of Hydra.

A. RF/Baseband Hardware Specification

Table I lists the relevant characteristics of the Hydra system hardware for the experiments in this paper. The operating frequency was placed at the upper edge of the 2.45 GHz industrial, scientific, and medical (ISM) band, above all interference observed by the spectrum analyzer during the experiment [18]. The choice of this frequency is relevant to IEEE 802.11n wireless LANs that will soon occupy this spectrum with beamforming-capable physical layers. The bandwidth of operation is 1 MHz compared to the 20 MHz

or 40 MHz bandwidths that 802.11n LANs operate on. For this experiment, the bandwidth is not of considerable importance since, with the exception of ultrawideband (UWB) channels, coherence time statistics are not dependent on the bandwidth of operation [20]. The maximum transmit power is listed as 10 mW, but in order to maintain linearity at the transmitter, typical operation was below 7.5 mW. Custom L-shaped copper microstrip antennas were chosen over off-the-shelf commercial WLAN antenna products because of their desirable S_{11} reflection coefficient characteristics, which fell below -20 dB for the entire spectrum of operation.

B. Software Architecture

Hydra features a completely software-defined protocol architecture that runs on a general purpose processor. The physical layer code is implemented using GNU Radio [21]. This open-source software allows developers to implement modular signal processing blocks in C++ and flexibly connect them together using python as a glue language. The community of users and developers for these software packages is broad, ranging from amateur radio and networking enthusiasts to experienced university and industry researchers. Although not utilized in the experiments of this paper, Hydra also features implementations for MAC, network, and an interface to TCP/IP applications using Click [22].

C. Physical Layer Algorithms

Hydra follows the IEEE 802.11 MIMO-OFDM PHY as provided by *Task Group N* in its Draft 2.0 Standard [23]. The orthogonal frequency division multiplexing (OFDM) modulation in this physical layer provides efficient equalization of frequency selective fading. Moreover, the MIMO algorithms in the standard allow for a framework to perform space-time processing techniques along with feedback functionality. Both of these features along with all the components found in traditional PHYs, make its implementation desirable for commercial products and experimentation alike. This physical layer simplified the design process considerably for the experiments in this paper.

Conforming with the 802.11n physical layer, blocks of binary data, that we shall denote *packets*, are transmitted inside a *frame*. This frame format, as illustrated in Figure 1 (a), serves many purposes. First, the training sequences in the packet allow for asynchronous frame detection. Second, the training sequences allow for measurement of impairments, such as frequency offset, and relevant parameters, such as the wireless channel impulse response for channel equalization. The data payload is a waveform expression of the binary packet. The parameters used to map the binary packet to a continuous waveform are encoded in the header of the frame.

All of the above components of the frame are exactly as specified by the 802.11n PHY standard. The only non-standard component used in this experiment is the Extended Training. As mentioned earlier, the training sequences in the frame can be used for channel impulse response estimation. This is necessary to perform proper equalization of the distortion effects of the wireless channel. Unfortunately, transmission

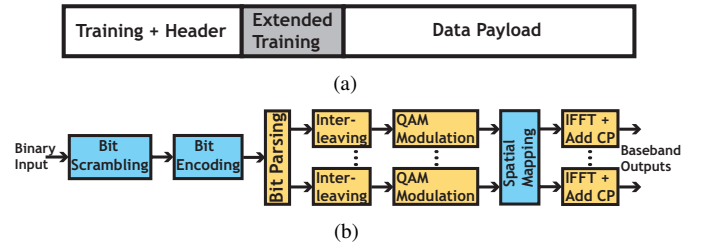


Fig. 1. IEEE 802.11n frame format (a) and transmit processing (b)

schemes, such as beamforming, become part of the *effective* wireless channel. That means that CSI feedback from channel estimates of this training no longer represent the channel of interest, but a beamformed version of that channel. The 802.11n standard provides a method for extracting the true channel from the beamformed version of the channel. Preferring simplicity over efficiency, Hydra was designed so that extra training information was sent in each frame without any beamforming, or more generally (as we shall see later) without spatial mapping. In the experiments, the Extended Training field provided the CSI feedback as well as the non-beamformed SNR estimates for comparing beamforming and cyclic delay diversity.

The structure of the 802.11n PHY transmitter, as implemented in Hydra, is shown in Figure 1 (b). For the purposes of constructing a mathematical system model of the experiments, the key component of the transmission structure is the spatial mapping block. Let $\mathbf{x}_k^{l,m} = [x_{1,k}^{l,m}, x_{2,k}^{l,m}, \dots, x_{N_{STS,k}}^{l,m}]^T$ represent the input to the spatial mapping block where $x_{i,k}^{l,m} \in \mathbb{C}$, for the k th subcarrier of the l th OFDM symbol in packet m , and N_{STS} is the number of space-time-streams (or distinct streams) in the MIMO signal. Since the main function of the system model is for representation of the transmission strategies, the actual OFDM symbol and packet specified are irrelevant. In other words, the system model holds *equally* for all OFDM symbols in all packets. Therefore, the l,m notation is dropped and $x_{i,k}^{l,m} = x_{i,k}$ for the remainder of the paper. The spatial mapping function $s(\bullet)$ maps the complex vector of dimension N_{STS} to a complex vector of dimension N_{TX} , $s : \mathbb{C}^{N_{STS}} \rightarrow \mathbb{C}^{N_{TX}}$, where N_{TX} is the number of transmit antennas. Given that the feedback transmission strategies will not include spatial multiplexing or space-time block coding, it can be assumed throughout the remainder of this paper that $N_{STS} = 1 \Rightarrow \mathbf{x}_k = x_{1,k} \triangleq x_k$. Furthermore, the spatial mapping function is restricted to the space of linear functions such that $s(\mathbf{x}_k) = \mathbf{Q}_k \mathbf{x}_k = \mathbf{q}_k x_k = \tilde{\mathbf{x}}_k$, where $\tilde{\mathbf{x}}_k$ is the spatially mapped output and $\mathbf{Q}_k \in \mathbb{C}^{N_{TX} \times N_{STS}}$ is the spatial mapping matrix. Several transmit diversity strategies can be packaged into this matrix framework, including digital beamforming (BF) and cyclic delay diversity (CDD) [24], both of which will be revisited after the Hydra receiver is discussed.

The receiver structure is displayed in Figure 2. Like the transmitter, the key component of the receiver involves spatial mapping, in this case extracting an estimate $\hat{\mathbf{x}}_k$ of the k th subcarrier in each OFDM symbol. This estimate of \mathbf{x}_k follows

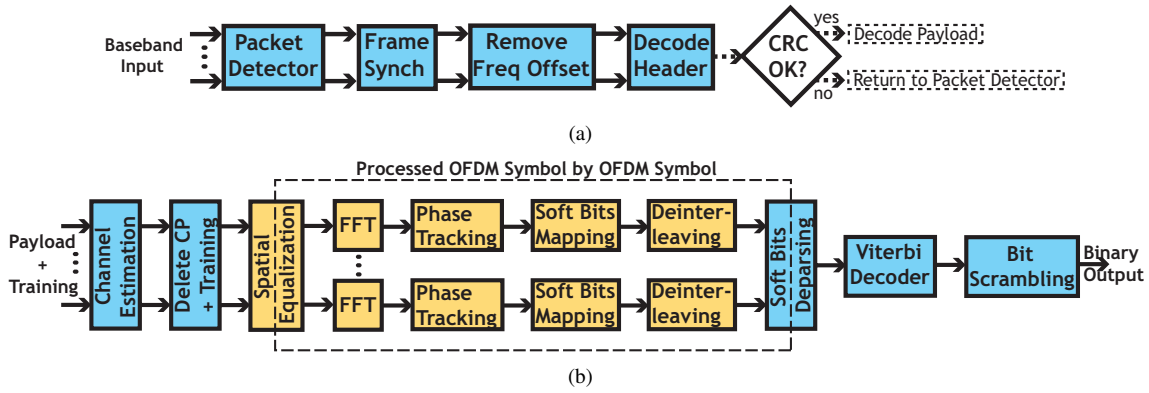


Fig. 2. Hydra receiver synchronization (a) and data processing (b)

the combination of the spatial equalization and FFT blocks in Figure 1. If frequency domain equalization is performed, this obviates the need for an explicit FFT operation after the spatial equalization. In a sense, the Spatial Equalization block is the inversion of the combination of the wireless channel and the spatial mapping block. It is assumed that, by using OFDM, the wireless channel impulse response experienced by each sub-carrier is frequency flat. Additionally, the model assumes that the coherence time of the wireless channel impulse response is large enough such that each packet observes a constant channel over the duration of waveform transmission. Both of these assumptions are often accepted for indoor channels [20]. Hence, let $\mathbf{H}_k \in \mathbb{C}^{N_{RX} \times N_{TX}}$ represent the complex baseband frequency flat impulse response of the wireless channel for OFDM subcarrier k . Effectively, the spatial equalization block receives \mathbf{y}_k and maps it with function $r(\bullet)$ to $\hat{\mathbf{x}}_k$. If we also assume that the receiver is linear, then $r(\mathbf{y}_k) = \mathbf{G}_k^H \mathbf{y}_k = \mathbf{g}_k^H \mathbf{y}_k$, where $\mathbf{G}_k \in \mathbb{C}^{N_{RX} \times N_{STS}}$. Note again that $\hat{\mathbf{x}}_k = \hat{x}_{1,k} = \hat{x}_k$ since $N_{STS} = 1$. It is now possible to create the complex baseband system model representing the input and output of the effective channel (combined spatial mapping and wireless channel). Thus,

$$\hat{x}_k = (\mathbf{g}_k^H \mathbf{H}_k \mathbf{q}_k) x_k \quad (1)$$

may be used to represent cyclic delay diversity, digital beamforming, limited-feedback beamforming and equalization methods.

Cyclic delay diversity is a simple, yet effective method for achieving full diversity order without knowledge of the wireless channel impulse response at the transmitter. By applying a discrete-time, per-transmit-antenna circular shift to each OFDM symbol it is possible to translate the spatial diversity experienced by multiple transmit antennas into frequency diversity. For bit-interleaved and coded OFDM systems, see Figures 1 and 2, the forward error correction over the frequency subcarriers provides all that is necessary to exploit the frequency diversity created in the wireless channel. OFDM symbols preserve the properties of the discrete Fourier transform (DFT) by adding a cyclic prefix. Therefore, by exploiting the equivalence of the discrete-time and discrete-frequency domains it is possible to implement cyclic delay diversity in the frequency domain. Moreover, using the circular time shift property of the DFT, cyclic delay diversity is easily

placed in the spatial mapping framework. It follows that the spatial mapping vector of cyclic delay diversity, for each scalar element of \mathbf{q}_k^{CDD} ,

$$q_{i,k}^{CDD} \triangleq \exp \left\{ \frac{-j2\pi k N_{i,CS}}{N_{DFT}} \right\} \quad (2)$$

where N_{DFT} is the block size of the DFT and $N_{i,CS}$ is the number of discrete-time symbols to be circularly shifted on transmit antenna i [25].

Digital beamforming, using channel state information feedback, attempts to transmit all of the energy over the maximum eigenmode of the effective channel $\mathbf{g}_k^H \mathbf{H}_k \mathbf{q}_k$. If we jointly optimize transmission over all transmit spatial mapping matrices (beamforming vectors), \mathbf{q}_k , and receive combining vectors, \mathbf{g}_k , then the optimal solution in terms of maximizing the effective channel total energy follows from the singular value decomposition of the channel matrix, $\mathbf{H}_k = \mathbf{U}_k \mathbf{S}_k \mathbf{V}_k^H$, where \mathbf{U}_k and \mathbf{V}_k are unitary matrices and \mathbf{S}_k is a diagonal matrix of dimension $\min\{N_{TX}, N_{RX}\}$. Hence, assuming the diagonal elements of \mathbf{S}_k are sorted by descending amplitude, the optimal beamforming vector is

$$\mathbf{q}_k^{BF} \triangleq [\mathbf{V}_k]_{:,1} \quad (3)$$

and the corresponding optimal combining vector

$$(\mathbf{g}_k^{BF})^H \triangleq [\mathbf{U}_k^H]_{1,:} \quad (4)$$

provides the maximum energy effective channel response.

Limited feedback beamforming reduces the overhead of transmitting the complete CSI over the feedback channel. By creating finite-size codebook with a specified bit-precision, feedback can drastically be reduced using the beamforming codeword index instead of the codeword itself. There exist several ways to construct the codebook including vector quantization [8] and Grassmanian subspace packing [5]. In this paper the latter codebook is chosen with 32 elements (5-bit precision). Larger codebooks can be chosen, but do not necessarily observe a performance improvement [3]. Assigning \mathbf{W}_{32} the notation for the Grassmanian codebook with 32 elements,

$$\mathbf{q}_k^{LFBF} \triangleq \arg \min_{\mathbf{q}_k \in \mathbf{W}_{32}} \|\mathbf{q}_k - \mathbf{q}_k^{BF}\|_2 \quad (5)$$

and

$$\mathbf{g}_k^{LFBF} \triangleq \frac{\mathbf{H}_k \mathbf{q}_k}{\|\mathbf{H}_k \mathbf{q}_k\|_2} \quad (6)$$

using (4) above assuming that \mathbf{q}_k^{LFBF} approximates the dominant right singular vector of \mathbf{H}_k .

As a note of clarification, the combining vectors in (4) and (6) are not explicitly used in spatial equalization at the receiver. Instead, maximal ratio combining (MRC) is used in combination with the beamforming vectors and cyclic delay diversity. Maximal ratio combining, although not necessary, solves the optimization problem $\mathbf{g}_k^{MRC} = \arg \max_{\mathbf{g}_k \in \mathbb{C}^{N_{RX} \times 1}} \|\mathbf{g}_k^H \mathbf{H}_k \mathbf{q}_k^{(LF)BF}\|_2$ so that

$$\mathbf{g}_k^{MRC} \triangleq [\tilde{\mathbf{V}}_k]_{:,1} \quad (7)$$

using the SVD of the effective channel $\mathbf{H}_k \mathbf{q}_k^{(LF)BF} = \tilde{\mathbf{H}}_k = \tilde{\mathbf{S}}_k \tilde{\mathbf{V}}_k^H$. Therefore, MRC provides a general framework for optimal receiver performance for all transmission diversity schemes considered in this paper. Furthermore, since maximal ratio combining is based on the effective channel estimate at the receiver, feedback delay perturbs the combining vector from the SVD of the original channel and will no longer be optimal.

IV. EXPERIMENT DESCRIPTION

The experiments conducted in this paper were designed to measure a variety of statistics and metrics of our system that provide insight into the feedback delay problem. Correlation statistics of the wireless channel in our indoor office setting were measured to approximate the coherence time of this environment. Measurements of bit-error rate taken using different MIMO techniques provide a performance metric for comparing beamforming (with feedback delay) against an uninformed delay-diversity scheme. Finally, statistics for the distribution of codebook indices are taken to provide a mechanism for computing theoretical bounds on the performance of beamforming under feedback delay [1].

This section describes the experimental setup that was required in order to measure the above quantities. In particular, the mechanism for feedback, the statistics of our indoor wireless channel, the experimental procedure used, and the mechanism for collecting data will be discussed in this section.

A. Prototype Setup and Indoor Wireless Channel

In constructing an experiment to characterize the impact of feedback delay on beamforming, CSI from the receiver can be fed back to the transmitter using either in-band wireless communication or out-of-band communication through a wired or dedicated feedback channel. In practical wireless systems, CSI must be exchanged through in-band mechanisms using limited feedback or by using reciprocity assumptions. Sharing CSI over the unreliable wireless medium may degrade the performance of beamforming. To avoid the overhead and impact of this unreliable feedback method, this experiment was conducted using a low-latency and error-free wired feedback channel implemented over a TCP/IP connection between the transmitter and receiver. This out-of-band feedback method

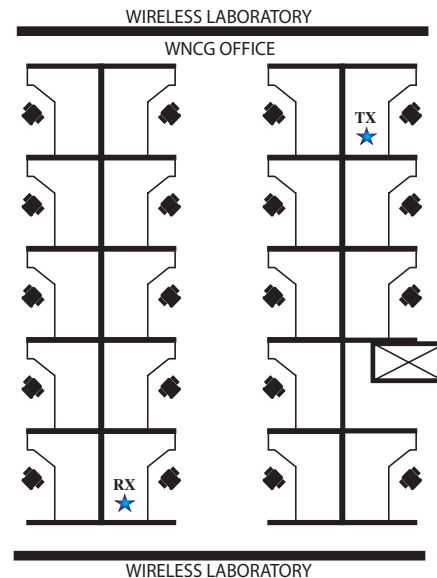


Fig. 3. Floor plan of indoor office setting for feedback beamforming experiment. The office has rows of cubicles, made with metal frames, and a large metal support column.

allows us to observe the impact of feedback delay independent of degradation caused by imperfect feedback. Note that this error-free feedback channel does not imply that the CSI fed back to the transmitter is perfect. In fact, this information is subject to estimation error caused by real world impairments such as synchronization error, frequency offset, or interference (impairments often overlooked in previous work on feedback delay) [1], [4].

The experiments in this paper were performed in the indoor office environment depicted in Figure 3. The transmitter and receiver, separated by a distance of 10 m, are located in two cubicles as might be the case in typical indoor office usage. As discussed in [1], the impact of feedback delay depends on the coherence time of the wireless channel. These statistics of the wireless channel are entirely dependent on the effective doppler of the environment. At a carrier frequency of 2.5 GHz, this doppler is determined by the motion of objects larger than 12.0 cm. In the absence of movement in the environment, the wireless channel will remain static as the electromagnetic propagation in the environment does not change. The wireless channel in such a static environment remains highly correlated for hundreds of seconds, as verified through measurement in an empty office. To produce meaningful results, it is necessary to create a fading channel with stationary (or at least nearly stationary) correlation statistics. In order to create such a fading channel the antennas of each node were mounted on oscillating fans (on the body of the fan, not on the rotating blades). The two fans used in this experiment oscillated with periods of 13.75 seconds and 11.25 seconds respectively. Since these fans were unsynchronized and had different periodicity, the effective wireless channel created by this setup had a pseudo-random fading pattern that would recombine only after a very long period (determined by the greatest common denominator of the fans' periods). This approach was necessary since moving large objects around

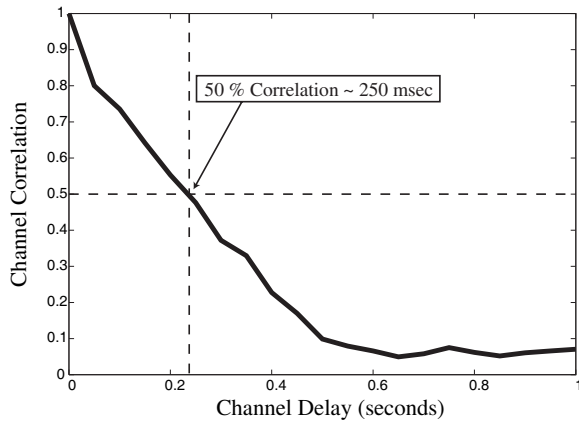


Fig. 4. Measured channel correlation statistics for indoor wireless channel. Coherence time is approximately 250 msec.

the office to create the desired doppler was not feasible.

Measuring correlation statistics using the fading channel mentioned required gathering channel measurements. Channel sounding was performed using repeated transmission of null packets (i.e. packets containing only the IEEE 802.11n training sequence and header). When performing channel sounding using this type of packet-based approach it is important to consider the impact of phase offset introduced by the crystal oscillator at the transmitter. The initial phase of the oscillator, which is unknown at the time of sounding, imparts a constant phase offset to each component of the channel matrix and can obscure the actual correlation statistics of the channel. After normalizing the phase of the channel measurements to correct for this often neglected feature of real systems, the correlation statistics computed from this data, shown in Figure 4, indicates that the coherence time of our indoor office setting is approximately 250 milliseconds. This corresponds to other indoor wireless channel measurements in the literature [16], [26].

B. Experiment Procedure

The goal of the experiment conducted in this paper is to characterize the tradeoff between throughput and feedback delay using beamforming in a practical wireless system. In order to design an effective experiment, special care was taken to ensure that feedback delay was accurately produced and that CSI contained minimal estimation error. The procedure used in conducting the feedback experiments for this paper is described below.

- P0:** Pick a transmit power P_{TX} as a random number with uniform distribution $P_{TX} \sim \mathcal{U}[P_{TX_{min}}, P_{TX_{max}}]$.
- P1:** Transmit a packet using CDD, i.e. without feedback at transmit power P_{TX} for baseline comparison.
- P2:** Wait for 50 msec to allow receive processing to complete.
- P3:** Transmit a sounding packet at maximum transmit power to reduce estimation error in the estimate of the full MIMO channel.
- P4:** Wait for desired delay minus some ϵ time to account for processing delay and properly age feedback information.

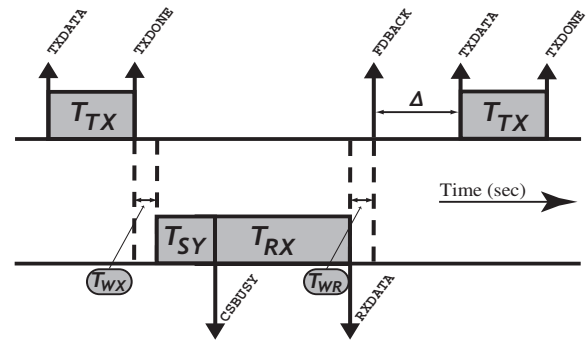


Fig. 5. Feedback delay construction with sounding packets; vertical arrows indicate timestamps, boxes indicate processing time at the transmitter or receiver, and circles point to times related to waveform transmission

- P5:** Transmit a packet using beamforming at transmit power P_{TX} . The beamforming vector is generated using CSI obtained over the wired feedback channel.
- P6:** Repeat steps **P4** and **P5** for additional feedback delays.
- P7:** Repeat steps **P0-P6** as needed to achieve desired precision in BER statistics over SNR range of interest.

The procedure above was performed for a variety of coding and modulation schemes. For each data rate, the impact of feedback delay can be measured effectively only over a specific SNR range. Capacity vanishes below this range, and BER becomes very small above this range. As such, $P_{TX_{min}}$ and $P_{TX_{max}}$ are tuned appropriately for each data rate to ensure operation in the desired SNR range. It is important to note that even though beamforming packets have variable transmit power, sounding packets are always transmitted at the maximum transmit power in the linear region of the transmit amplifier. This reduces the chance that channel estimation error adversely impacts beamforming. In order to reduce the impact of errors introduced by phase tracking, short packets were transmitted in all of the experiments. Lower data rates, which have less data bits per OFDM symbol, required smaller packets. Thus, in order to obtain accurate measurements at lower data rates, more iterations were performed.

In software defined radios implemented on general purpose processors, as in this experiment, processing delays are subject to the variability of schedulers and multi-threaded operating systems. In order to implement accurate feedback delays on such a system it is critical to use proper timestamping for sounding and feeding back data (steps **P3-P5**). This procedure is illustrated in Figure 4. At time TXDATA, the transmitter initiates the transmission of a sounding packet, which after processing time T_{TX} is transmitted over the air at time TXDONE. After over the air time transmission time T_{WX} , the receiver synchronization algorithm detects a packet at time CSBUSY. Then after some receive processing time T_{RX} , the data is fed back to the transmitter, incurring a wired feedback delay of T_{WR} . The receive processing time T_{RX} greatly dominates T_{WX} , T_{SY} , and T_{WR} and thus is an accurate measure of the feedback delay of the system. The receiver piggybacks T_{RX} along with the CSI on its feedback communication. At the transmitter the feedback information

is aged for an additional pause time Δ , such that

$$\Delta = (\text{FDBACK} - \text{CSBUSY} - T_{TX}). \quad (8)$$

After this procedure (i.e. sounding, wired feedback over TCP/IP, and feedback aging), the transmitter can use the uncompressed MIMO CSI to compute optimal beamforming vectors, or quantize it and then compute limited feedback beamforming vectors which are then used in the transmission of step **P5**. In the case where feedback is not available due to a dropped sounding packet (usually because of synchronization error), all subsequent packets will be sent using CDD until new feedback becomes available. In addition to timestamping events mentioned in this section, extensive data logging of channel information, coded and uncoded bits, and feedback data provided an abundance of data used to debug and extract a clear picture of the events in each experimental test.

V. RESULTS AND ANALYSIS

This section presents both the results and analysis of limited feedback beamforming and CSI delay experiments. These experiments use the physical layer algorithms of Section III and the setup procedure in Section IV. By careful extraction of the bit-error-rate curves (BER) from the decoded packets for different modulation and coding schemes, this section reveals the throughput gain for 50 msec delayed limited feedback beamformed packets versus cyclic delay diversity packets. A throughput gain versus feedback delay trend was also observed for feedback delay up to 1 second. Not only do these measurements demonstrate the capacity gain of limited feedback beamforming, but they also accurately characterize the capacity gain as a function of feedback delay.

A. Throughput Gain Results

Previous theoretical analysis has shown that, under certain channel assumptions, there exists an upper bound on the capacity gain, $\Delta\mathcal{C}(D)$, that limited-feedback beamforming provides (versus capacity of transmitter without CSI). Explicitly,

$$\Delta\mathcal{C}(D) \triangleq \mathcal{C}_{BF}(D) - \mathcal{C}_{UI} \quad (9)$$

for uniformed transmitter capacity \mathcal{C}_{UI} and limited feedback beamforming capacity \mathcal{C}_{BF} as a function of delay D . Unfortunately, system capacity is not necessarily easily translated into realizable system performance. Past work has shown that, for a fixed bit-error-rate, QAM constellations exhibit a constant SNR (in dB) gap from capacity [27]. Therefore, by transmitting QAM constellations and selecting the proper constellation order and convolutional coding rate, it is possible to maintain a relatively static bit error rate and thus, approximate the capacity trend. Since the capacity of the wireless channel in this experiment is unknown, we measure the impact of feedback delay by observing the throughput of limited feedback beamforming and cyclic delay diversity. For a single spatial stream, Table II shows the modulation and coding schemes (MCS) available in 802.11n. For the Hydra physical layer we define throughput as

$$T_{MCS,i}(\text{SNR}) \triangleq \mathcal{R}_i(1 - \text{BER}_i(\text{SNR})) \quad (10)$$

TABLE II
IEEE 802.11N MCS FOR SINGLE SPATIAL STREAM

MCS	QAM Order	Coding Rate	Total Rate (\mathcal{R}) ($\frac{bps}{Hz}$)
0	BPSK	1/2	0.50
1	QPSK	1/2	1.00
2	QPSK	3/4	1.50
3	16-QAM	1/2	2.00
4	16-QAM	3/4	3.00
5	64-QAM	2/3	4.00
6	64-QAM	3/4	4.50
7	64-QAM	5/6	5.00

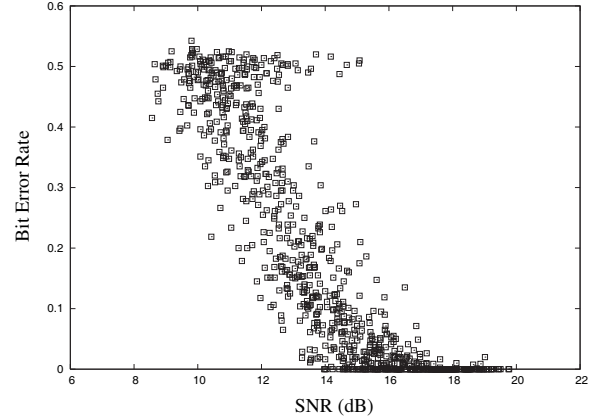


Fig. 6. Scatter plot of MCS 4 of experimental data

where \mathcal{R}_i , BER_i are the total rate and bit error rate for MCS i , respectively. Using this definition of throughput we further define *throughput gain*, $\Delta\mathcal{T}(D)$, for limited-feedback beamforming as,

$$\Delta\mathcal{T}(D) \triangleq \mathcal{T}_{BF}(D) - \mathcal{T}_{CDD} \quad (11)$$

for limited-feedback beamforming throughput \mathcal{T}_{BF} and cyclic delay diversity throughput \mathcal{T}_{CDD} . Cyclic delay diversity is used as a baseline comparison for uninformed transmission. Cyclic delay diversity provides full diversity order without any additional receiver processing. Using the frequency domain spatial mapping framework from Section III it is shown that cyclic delay diversity is a special case of transmit beamforming. Other spatial diversity techniques were considered for baseline comparison such as space-time block coding, however, these methods require additional receiver processing without added diversity gain.

In order to calculate the throughput curve for limited feedback beamforming and cyclic delay diversity, it is necessary to define the switching points between the different QAM constellation orders and convolutional coding rates. Instead of profiling the Hydra system to discover the proper switching points, a simpler experimental procedure was performed. The bit-errors in each MCS were measured for 1000 packets over a range of SNR that covered the transition regions of the throughput curve. This results in a scatter plot of bit-errors per packet versus SNR measured from the extended training. An example for MCS 4 can be observed in Figure 6. The SNR values were binned to small intervals and the BER was averaged over each bin. This BER versus SNR curve for MCS

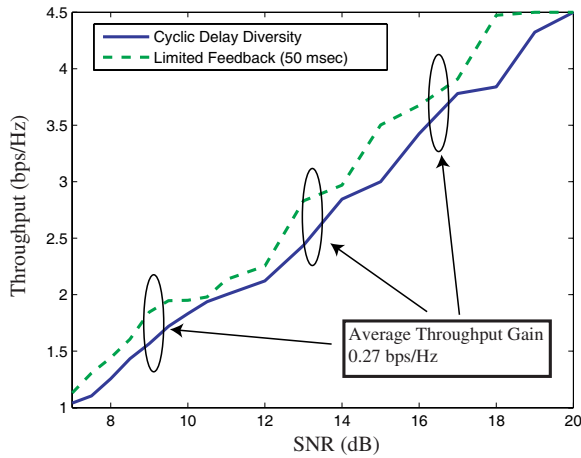


Fig. 7. Throughput versus SNR for limited feedback beamforming with 50 msec feedback delay and cyclic delay diversity

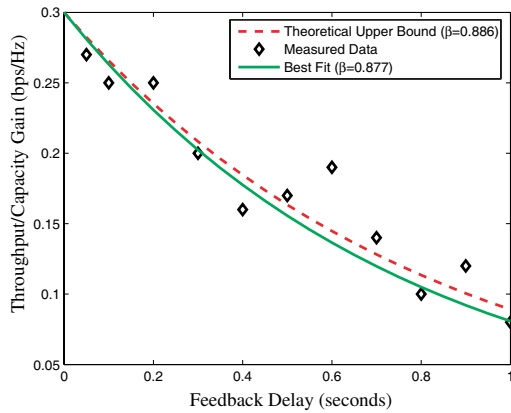


Fig. 8. Throughput gain versus feedback delay for limiting feedback beamforming and 5-bit codebooks

i was translated into throughput using equation (10). Through visual inspection, the correct SNR regions were observed for each MCS. Finally, to make the first and second order derivatives of the throughput function continuous, a cubic splines interpolation procedure was processed over the data. Figure 7 demonstrates the throughput calculation for limited feedback beamforming in a 5-bit codebook with 50 msec feedback delay and cyclic delay diversity.

Throughput curves were generated for 100 – 1000 msec feedback delay over all the MCS. In order to compare with theoretical feedback delay effects from [1], the throughput gain was calculated using (11) as an approximation of (9). The resulting throughput calculations are displayed in Figure 8. Also included in this graph, and as discussed in detail in the next subsection, is the theoretical upper bound from [1].

B. Performance Analysis

Figures 7 and 8 reflect a comprehensive measurement on the effect of feedback delay and its impact on system throughput. For system design, it is desirable to characterize the expected performance loss caused by aging feedback. Moreover, insight gained from the feedback delay characterization may

potentially allow for more intelligent limited feedback codebook construction [28], [29] and suggest how often channel feedback needs to be refreshed for beamforming to perform effectively.

Figure 7 observes the throughput gain of limited feedback with 50 msec delay versus cyclic delay diversity for a baseline comparison. As expected, limited feedback beamforming improves the performance of the system over all SNR. Since the coherence time of the wireless channel was observed to be approximately 250 msec, a 50 msec delay should be very close to the maximum achievable throughput gain. The throughput gain is averaged over 7 – 22 dB SNR to yield 0.27 bps/Hz. This result is smaller than expected [8], since theoretically beamforming provides a 3 dB SNR improvement in Rayleigh fading channels [30]. Experimental results display degraded performance, however, because of impairments not observed in typical wireless channel models. This can include frequency offset, synchronization error, phase noise, channel estimation error, and nonlinearities in hardware components.

The principle contribution of this experiment is shown in Figure 8. This figure displays the loss in throughput versus feedback delay. Analytical results from [1] show that the capacity gain as a function of feedback delay can be bounded by an exponential function. Specifically,

$$0 \leq \Delta C(D) \leq \alpha \beta^D \quad (12)$$

for scalar constants $\alpha, \beta \in \mathbb{R}$ and $D \in \mathbb{N}$ the normalized delay. D is the number of state transitions taken in a Markov process that models the temporal correlation of the wireless channel. α refers to the capacity gain of limited feedback beamforming with zero feedback delay. β is the second largest eigenvalue of the transition probability matrix which describes the evolution of the wireless channel through quantized codebook space. For example in our limited feedback beamforming experiment, we measure the state of the channel every 50 msec. Each 50 msec step corresponds to an increment of D . The transition probability matrix corresponds to the conditional probability that the quantized limited feedback beamforming vector switches between any two codebook indices.

In Figure 8, the measured data represents the observed throughput gain as a function of feedback delay. Using an exponential fit to the measured data with $\alpha = 0.3$, the least squares solution for the exponential term yields $\beta = 0.877$. Additionally, by collecting statistics on the transitions of the indices of the quantized codebook we were able to reconstruct the transition probability matrix. This transition probability matrix provides $\beta = 0.886$ from the 2nd largest absolute eigenvalue. Therefore, we have two results that characterize capacity (throughput) gain as an exponential function of the feedback delay. The first result was obtained through exhaustive throughput measurements over various SNR, feedback delay, and MCS. The second result, however, only required collecting statistics at a single SNR and feedback delay (50 msec) to compute the transition probability matrix. Although the second result theoretically represents an upper bound on the capacity (throughput) gain as a function of delay, this upper bound accurately approximates the capacity (throughput) gain that we observed. Hence, this simple calculation on the upper

bound of the capacity (throughput) gain has been verified both analytically [1] and experimentally to closely follow the actual results.

VI. CONCLUSION

In this work we have characterized the impact of feedback delay on the performance of limited feedback beamforming through measurements in real wireless channels. These measurements were obtained on a IEEE 802.11n draft 2.0 standard MIMO-OFDM prototype. In addition, we present the methodology and procedure for conducting these feedback experiments. The measurement of throughput gain versus feedback delay in this experiment verifies the accuracy of analytically derived performance bounds [1]. Furthermore, verifying these results suggests a simple procedure to characterize the performance of feedback delay in limited feedback beamforming without exhaustive throughput measurements.

VII. ACKNOWLEDGEMENTS

The authors would like to thank Takao Inoue for generating the Grassmannian codebooks for the experiments. We would also like to thank Kaibin Huang for his many useful discussions on feedback delay effects.

REFERENCES

- [1] K. Huang, B. Mondal, R. W. Heath, Jr., and J. G. Andrews, "Effect of Feedback Delay on Multiple-Antenna Limited Feedback for Temporally-Correlated Channels," in *Proceedings of IEEE Global Telecommunications Conference 2006*, October 2006, pp. 1–5.
- [2] T. K. Y. Lo, "Maximum Ratio Transmission," *IEEE Trans. on Communications*, vol. 47, pp. 1458–1461, October 1999.
- [3] D. J. Love and R. W. Heath, Jr., "Equal Gain Transmission in Multiple-Input Multiple-Output Wireless Systems," *IEEE Trans. on Communications*, vol. 51, pp. 1102–1110, July 2003.
- [4] D. J. Love, R. W. Heath, Jr., W. Santipach, and M. L. Honig, "What Is the Value of Limited Feedback for MIMO Channels?" *IEEE Communications Magazine*, vol. 42, pp. 54–59, October 2004.
- [5] D. J. Love, R. W. Heath, Jr., and T. Strohmer, "Grassmannian Beamforming for Multiple-Input Multiple-Output Wireless Systems," *IEEE Trans. on Info. Theory*, vol. 49, pp. 2735–2747, October 2003.
- [6] K. K. Mukkavilli, A. Sabharwal, E. Erkip, and B. Aazhang, "On Beamforming With Finite Rate Feedback in Multiple-Antenna Systems," *IEEE Trans. on Info. Theory*, vol. 10, pp. 2562–2579, October 2003.
- [7] V. K. N. Lau, Y. Liu, and T.-A. Chen, "Optimal Partial Feedback Design for MIMO Block Fading Channels with Feedback Capacity Constraint," in *IEEE International Symposium on Information Theory 2003*, June 2003, p. 65.
- [8] B. Mondal and R. W. Heath, Jr., "Performance Analysis of Quantized Beamforming MIMO Systems," *IEEE Transactions on Signal Processing*, vol. 54, pp. 4753–4766, December 2006.
- [9] H. T. Nguyen, J. B. Andersen, and G. F. Pedersen, "Capacity and Performance of MIMO Systems under the Impact of Feedback Delay," in *Proceedings of IEEE International Symposium on Personal, Indoor and Mobile Radio Communications 2004*, vol. 1, September 2004, pp. 53–57.
- [10] J. Du, Y. Li, D. Gu, A. F. Molisch, and J. Zhang, "Estimation of Performance Loss Due to Delay in Channel Feedback in MIMO Systems," in *Proceedings of IEEE Vehicular Technology Conference 2004*, vol. 3, September 2004, pp. 1619–1622.
- [11] T. A. Thomas, "Transmit Beamforming Weights for Channel Estimation Error and Feedback Latency in OFDM," in *Proceedings of IEEE International Conference on Acoustics, Speech, and Signal Processing*, vol. 3, April 2007, pp. III–429–III–432.
- [12] M.-S. Alouini and A. Goldsmith, "Adaptive Modulation over Nakagami Fading Channels," *Kluwer Journal on Wireless Communications*, vol. 13, no. 1-2, pp. 119–143, May 2000.
- [13] Y. Kakishima, H. Le, S. H. Ting, K. Sakaguchi, and K. Araki, "Experimental Analysis of MIMO-OFDM Eigenmode Transmission with MMSE Interference Canceler," in *Proceedings of IEEE International Symposium on Personal, Indoor and Mobile Radio Communications 2006*, September 2006, pp. 1–5.
- [14] K. Kobayashi, T. Ohtsuki, and T. Kaneko, "MIMO Systems in the Presence of Feedback Delay," in *Proceedings of IEEE International Conference on Communications 2006*, vol. 9, June 2006, pp. 4102–4106.
- [15] D. Li and X. Dai, "On the performance of MIMO-OFDM Beamforming Systems with Feedback Delay," in *International Conference on Wireless Communications, Networking and Mobile Computing 2006*, September 2006, pp. 1–4.
- [16] K. Mandke, R. C. Daniels, S.-H. Choi, S. M. Nettles, and R. W. Heath, Jr., "Physical Concerns for Cross-Layer Prototyping and Wireless Network Experimentation," in *Proceedings of the Second ACM International Workshop on Wireless Network Testbeds, Experimental Evaluation and Characterization*, 2007.
- [17] "GNU radio: Universal software radio peripheral radio." [Online]. Available: <http://www.comsec.com/wiki?UniversalSoftwareRadioPeripheral>
- [18] K. Mandke, S.-H. Choi, G. Kim, R. Grant, R. C. Daniels, W. Kim, S. M. Nettles, and R. W. Heath, Jr., "Early Results on Hydra: A Flexible MAC/PHY Multihop Testbed," in *Proceedings of the 65th IEEE Vehicular Technology Conference*, Apr. 2007, pp. 1896–1900.
- [19] "Hydra: A mimo-ofdm multihop wireless network prototype." [Online]. Available: <http://hydra.ece.utexas.edu>
- [20] A. Goldsmith, *Wireless Communications*. Cambridge University Press, 2005.
- [21] "GNU software radio." [Online]. Available: <http://www.gnu.org/software/gnuradio/>
- [22] E. Kohler, R. Morris, B. Chen, J. Jannotti, and M. F. Kaashoek, "The Click modular router," *ACM Trans. Comput. Syst.*, vol. 18, no. 3, pp. 263–297, 2000.
- [23] *Wireless LAN Medium Access Control (MAC) and Physical Layer (PHY) Specifications - Draft 2.0: Enhancements for Higher Throughput*, Part 11 standard ed., IEEE 802.11n Working Group, February 2007.
- [24] A. Dammann and S. Kaiser, "Standard conformable antenna diversity techniques for OFDM and its application to the DVB-T system," in *Global Telecommunications Conference, 2001. GLOBECOM '01. IEEE*, vol. 5, 2001, pp. 3100–3105 vol.5.
- [25] G. Bauch, "Capacity optimization of cyclic delay diversity," in *Vehicular Technology Conference, 2004. VTC2004-Fall. 2004 IEEE 60th*, vol. 3, 2004, pp. 1820–1824 Vol. 3.
- [26] T. S. Rappaport and T. Rappaport, *Wireless Communications: Principles and Practice (2nd Edition)*. Prentice Hall PTR, December 2001. [Online]. Available: <http://www.amazon.fr/exec/obidos/ASIN/0130422320/citeulike04-21>
- [27] J. Cioffi, *Digital Communications*. Stanford University Course Reader, 2006.
- [28] K. Huang, B. Mondal, R. W. Heath, Jr., and J. G. Andrews, "Multi-antenna limited feedback for temporally-correlated channels: Feedback compression," *Proc. of IEEE Global Telecommunications Conf.*, 2006.
- [29] J. V. Raghavan, R. W. Heath and A. Sayeed, "Systematic codebook designs for quantized beamforming in correlated MIMO channels," *accepted to IEEE Journal on Sel. Areas in Comm.*, 2006.
- [30] A. Paulraj, R. Nabar, and D. Gore, *Introduction to Space-Time Wireless Communications*. Cambridge University Press, 2003.